Available online at www.sciencedirect.com
SCIENCE DIRECT®
Comput. Methods Appl. Mech. Engrg. 195 (2006) 94–109
Computer methods in applied mechanics and engineering
www.elsevier.com/locate/cma

Multiscale construction and large-scale simulation of structural fabric undergoing ballistic impact

T.I. Zohdi *, D. Powell

Department of Mechanical Engineering, 6195 Etcheverry Hall, University of California, Berkeley, CA 94720-1740, USA

Received 29 March 2004; received in revised form 18 October 2004; accepted 10 January 2005

Abstract

Certain classes of new lightweight structural fabric, primarily used for ballistic shielding, possess a multiscale structure constructed from microscale fibrils, which are bundled together to form yarn. The yarn are tightly woven into sheets. Since experimental ballistic tests for the evaluation, design and optimization of such materials are extremely expensive and time consuming, it is advantageous to develop models amenable to rapid computational methods. The purpose of the present work is to develop an efficient computational strategy in order to rapidly construct and numerically simulate multiscale representations of this class of materials. Large-scale simulations are presented to illustrate the potential of the approach in delivering realistic responses, involving dynamic penetration of a new lightweight structural fabric.

Keywords: Multiscale modeling; Structural fabric; Dynamics; Penetration

1. Introduction

There exist a wide range of applications for lightweight structural fabric. A particular application of interest is to protect flight critical structural components in aircraft, such as electrical lines, hydraulic lines, and fuel lines. However, for such materials to become successfully integrated in engineering designs, laborious testing of sheets of fabric undergoing high velocity impact is required. There exist a wide variety of such structural fabric, for example the well-known material Kevlar. The reader is referred to Roylance and Wang [29], Taylor and Vinson [32], Shim et al. [30], Johnson et al. [16], Tabiei and Jiang [31] Kollegal and Sridharan [17] and Walker [35] for overviews. One recently developed structural fabric is zylon, which is a

* Corresponding author. Tel.: +1 510 642 6834; fax: +1 510 642 6163.
E-mail address: zohdi@newton.berkeley.edu (T.I. Zohdi).

0045-7825/$ - see front matter © 2005 Elsevier B.V. All rights reserved.
doi:10.1016/j.cma.2005.01.011

polymeric material produced by the Toyobo Corporation [33]. In the upcoming analysis, although the specific material of interest is zylon, the multiscale description is general enough to be applicable to a wide class of other structural fabric, such as Kevlar or other aramid-based materials. Zylon has a multiscale structure constructed from polybenzoxale (PBO) microscale fibrils, which are bundled to form yarn, which are then tightly woven into sheets (Fig. 1). Since experimental ballistic tests for the evaluation of such materials are extremely expensive and time consuming, it is advantageous to develop models amenable to rapid computational methods. Furthermore, such computational methods can be used to design and *optimize* weight- and cost-efficient barriers with desired ballistic resistance.

1.1. Experimental observations

Experimental ballistic data on zylon has been recently become available. The typical amount of time taken for a single labor-intensive ballistic test is on the order of 60–90 min. In order to perform the experiments, ballistic sheets of zylon are cut with special scissors from a roll and clamped around a circular bar into a square holder. The two parts of this square frame are secured by 9.5 mm diameter hard-steel bolts via an aluminum strip acting as a continuous washer. After assembly, this unit is clamped in a vertical position to a heavy triangular support mounted on a 700 kg steel table in such a manner that impact would be produced at a predetermined location on the target as determined by a laser beam mounted on the gun centerline. The tests are executed by means of a custom-built 12.9 mm inside diameter powder gun with 20 mm thick high-strength steel barrel of 1.6 m length. This device is mounted by means of a rail frame on the same table as the target. The gun is capable of accommodating a 50 caliber shell into which the projectile is inserted. The projectile consists of a 12.7 mm diameter steel cylinder with a mass of 36 g, with an aspect ratio of 3:1, heat treated to a hardness of R_c60, and copper-coated to a thickness of 0.5 mils to reduce barrel wear. A blast shield is placed in front of the muzzle to prevent interaction of the powder gases with target material. A projectile and fragment catcher consisting of a rag-filled box is positioned beyond all final velocity measuring units. All tests are conducted inside an enclosed chamber that is evacuated during firing. The initial velocity of the projectile is determined from the time required to successively break two parallel laser beams 156 mm apart that are focused on two photodiodes, located 1.5 m in front of the target. The signals from the diodes initiate the start and stop modes of a Hewlett–Packard 5316 time interval meter. Final velocities are determined in three ways: (1) By the use of a digital video recording camera operating

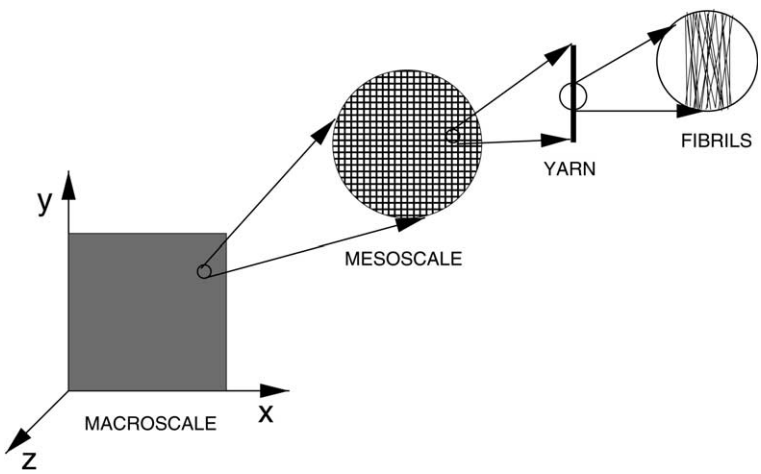

Fig. 1. A multiscale structural fabric representation.

at 10,000 frames/s, that captures the projectile position at a number of instances after the perforation using the dimensions of the projectile or a scale for distance determination; (2) By means of two silver-coated paper make-circuit grids spaced 50.4 mm apart, whose voltage pulses are directed to a time-interval meter and (3) two sets of 432×254 mm foils, with each pair separated by 12 mm and each set a distance of 12.7 mm apart, with the projectile contact providing a make-circuit for each set, allowing the respective signals to start and stop a time interval meter. A calibration curve has been established for initial velocity versus the amount of IMR 3031 powder placed in the shells. The number of desired sheets are cut and inserted in the target holder and the bolts were tightened with a 306 N-m torque wrench. Typical perforation patterns that such penetrators produce are shown in Fig. 2. Video clips of such tests and some preliminary data are available at http://www.me.berkeley.edu/compmat.

1.2. Objectives of this work

In order to numerically simulate tests, such as the one described in the previous section, a multiscale model, which is amenable to direct computation, is developed in this communication. The "building blocks" are yarn, comprised of one-dimensional microscale fibrils, which are arranged to form two-dimensional planar sheets of fabric (Fig. 1). A key aspect of such an approach is that if the properties of the fibrils are known, the structural scale properties can be constructed, without resorting to phenomenological parameters. For most types of structural fabric, the overall rupture of a single yarn is gradual, as opposed to abrupt, due to inhomogeneous microscale fibril failure, stemming from their the random misalignment, within the yarn. An important feature of the multiscale modeling approach is the ability to directly incorporate of fibril misalignment into the structural scale response of the fabric. An efficient numerical strategy is developed to rapidly construct and numerically simulate the multiscale system. Large-scale simulations are presented to illustrate the potential of the approach in delivering realistic responses, involving dynamic rupture and penetration of structural fabric.

The philosophy behind the proposed multiscale modeling approach is to harness the dramatic increases in readily available scientific computing to simulate realistic responses of structural fabric, by starting

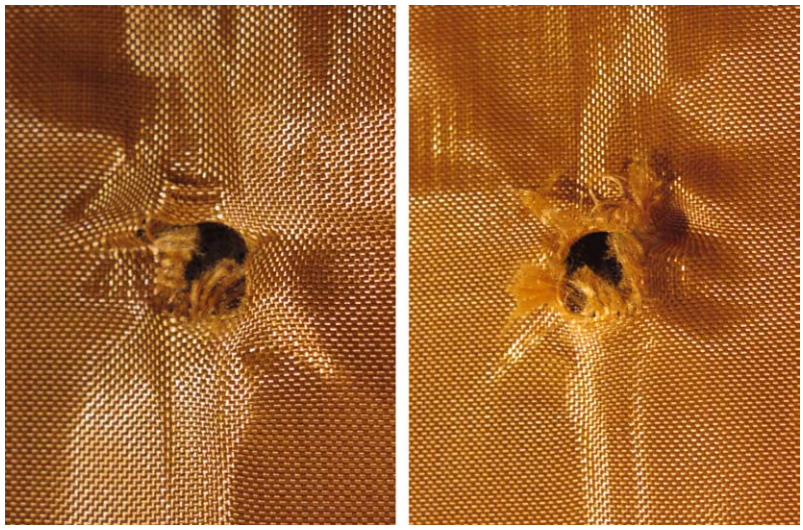

Fig. 2. Different pictures of highly localized holes resulting from the experimental shots, under the same conditions, conducted at UC Berkeley. In all cases the penetration was highly localized, with the resulting holes' diameters and cylindrical penetrator diameter being virtually identical.

directly at the microscale, where relatively simple descriptions of the material are possible. By employing enough of these simple structural elements, one can build an entire macroscale sheet of structural fabric, as shown in Fig. 1. The advantage is that relatively simple microscale models can be used, with the burden of the analysis being shifted to rapid efficient computation.

2. Multiscale construction of structural fabric

For structural fabric, a typical quantity of interest is the global, tensile, force-deflection response. The compressive response is usually of little interest, in particular if information on fabric rupture is sought. Therefore, analyses based on so-called relaxed theories of perfectly flexible solids are employed, which consist of enforcing a zero stress state for any compressive strains. Pipkin [28] appears to have been the first to have shown that such models are compatible with the conventional theory of elastic surfaces by considering a minimizing sequence for an associated variational problem, and that showing that such sequences have a structure similar to observed wrinkling in thin elastic sheets. This line of approach has been taken by several researchers for the elastostatic analysis of structural fabric; for example Buchholdt et al. [4], Pangiotopoulos [20], Bufler and Nguyen-Tuong [5] and Cannarozzi [7,6]. Steigmann and coworkers [34,12–14,1,2] have developed a series of theoretical results and elastostatic solution techniques based on pseudo-dynamic relaxation methods, such as those found in Papadrakakis [21]. Steigmann and coworkers have shown that a necessary condition for the existence of energy minimizers in elastostatics is for the structural members to carry no load in compression. This relaxed requirement is adopted for the microscale fibrils in the upcoming dynamic analyses, although, strictly speaking, it is only required in elastostatic cases.

We consider an initially undeformed two-dimensional network of yarn comprised of microscale fibrils (Fig. 1). The yarn are joined at the nodes, in other words, they are sutured together at those locations to form a network (Figs. 1 and 3).[1] The starting point for the analysis is a *purely one-dimensional* description of the tensile deformation of a microscale fibril. Since the fibrils are quite thin, one may assume a plane uniaxial-stress type condition. The axial strains, for structural fabric such as zylon, are expected to be on the order of 2–10%, in the elastic range, before rupturing.[2] Therefore, a relatively simple Kirchhoff-St. Venant material model is reasonable.

2.1. A single fibril

The stored energy of a single fibril is given by $W = \frac{1}{2}\mathbb{E}E^2$, where $\mathbb{E}$ is Young's modulus, where $E \overset{\text{def}}{=} \frac{1}{2}(C-1)$ is the Green–Lagrange strain, where $C \overset{\text{def}}{=} F^2$ is the right Cauchy–Green strain, where $F = \frac{\mathrm{d}x}{\mathrm{d}X}$ is the deformation gradient, where X are referential coordinates and where x are current coordinates along the axis of the filament. The second Piola–Kirchhoff stress is given by $S = \mathbb{E}E$. We remark that, during the calculations, it is convenient to work with quantities expressed in terms of the stretch ratio, $U = \frac{L}{L_o}$, where L is the deformed length of the fibril, L_o is its original length and, by virtue of a polar-decomposition, $E = \frac{1}{2}(U^2-1)$. *For this relaxed one-dimensional model*, the Cauchy stress, σ, is related to the second Piola–Kirchhoff stress by $\sigma = \frac{1}{J}F^2S$, where J is the Jacobian of F, $J = F$, thus $\sigma = FS$.

This relaxed (tensile-strain only, $F \geqslant 1$) one-dimensional model is polyconvex, which is a desirable (sufficient) property from a mathematical existence theory standpoint. Recall, a general three-dimensional stored energy function is polyconvex if, for two deformation gradients, $\boldsymbol{F}$ and $\boldsymbol{G}$

[1] In reality the yarn are tightly woven and that the nodes are the criss–cross contact junctions between the warp and the fill of the weave.

[2] For example, zylon ruptures at approximately a 3% axial strain [33].

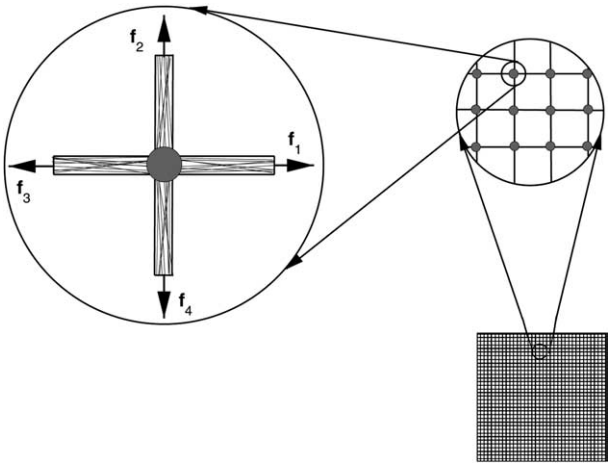

Fig. 3. Four yarn intersecting at a lumped mass (sutured-point).

$$W(\theta(\boldsymbol{F},\operatorname{cof}\boldsymbol{F},\det\boldsymbol{F})+(1-\theta)(\boldsymbol{G},\operatorname{cof}\boldsymbol{G},\det\boldsymbol{G}))\leqslant\theta W(\boldsymbol{F},\operatorname{cof}\boldsymbol{F},\det\boldsymbol{F})+(1-\theta)W(\boldsymbol{G},\operatorname{cof}\boldsymbol{G},\det\boldsymbol{G}), \tag{2.1}$$

where $\operatorname{cof}\boldsymbol{F}=\boldsymbol{F}^{-\mathrm{T}}\det\boldsymbol{F}$ and $0\leqslant\theta\leqslant 1$. In one-dimension, for tensile states only, the tensorial quantities take on the form $\boldsymbol{F}=F$, $\operatorname{cof}\boldsymbol{F}=1$ and $\det\boldsymbol{F}=F$. Thus, for the one-dimensional relaxed theory, convexity of $W(F)$ with respect to F is equivalent to polyconvexity. By computing two derivatives of $W(F)$, and enforcing $\frac{\partial^2 W}{\partial F^2}>0$ for convexity, we obtain

$$\frac{\partial^2 W}{\partial F^2}=\frac{\mathbb{E}}{2}(3F^2-1)>0, \tag{2.2}$$

which is valid for positive values of $\mathbb{E}$.

2.2. Behavior of yarn

Fibril misalignment at the micro-scale (Fig. 4) is unavoidable during the weaving process of materials such as zylon. However, misalignment is highly advantageous from the point of view of rupture resistance. The consequences of such misalignment are:

- The rupture of a yarn is not sudden, but rather gradual, due to the inhomogeneous rupture of the fibrils which comprise the single yarn.
- Due to the fact that the yarn are of finite thickness, with different random variations of the fibrils within each yarn, the material response is different from yarn to yarn. However, these differences are somewhat small for the size of yarn used in the analysis, as we shall see momentarily (Fig. 5).

In order to illustrate these effects, the responses for 10 yarn segments, gripped at the ends, each with a different random fibril realization, were computed, under displacement control. The results are shown in Fig. 5.[3] Each yarn contains approximately 350 fibrils. Also, according to the manufacturer, for a fibril,

[3] The orientation of the fibrils within the yarn where generated with a standard Fortran random number generator.

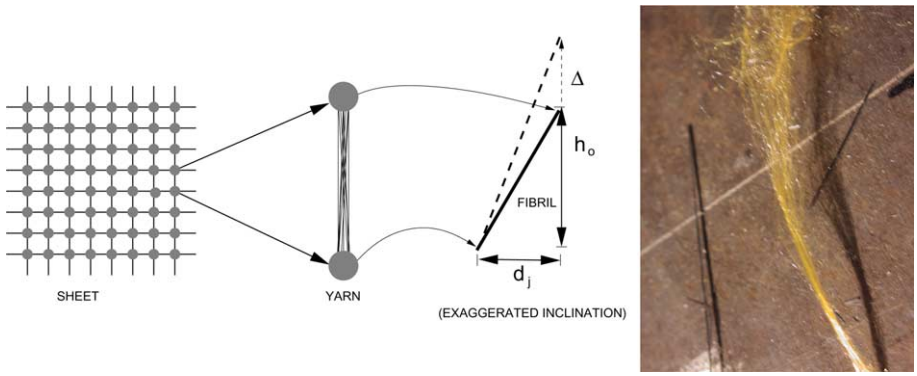

Fig. 4. Left: A zoom on an individual misaligned fibril. Right: A single zylon yarn.

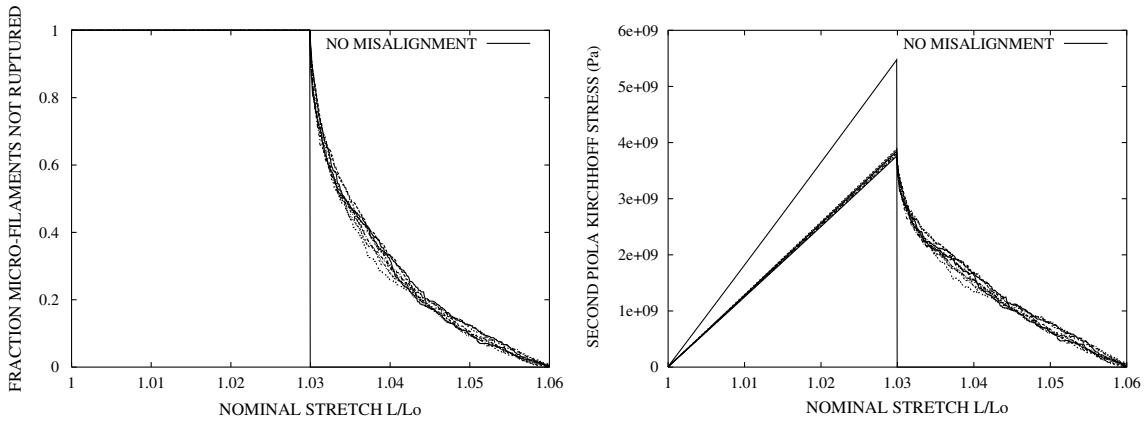

Fig. 5. Left: The fraction of fibrils that are *not ruptured* for 10 different yarn, each containing 350 fibrils. Right: The corresponding second Piola–Kirchhoff stress responses for the yarn.

$U_{\text{crit}} = 1.03$, and the Young's modulus is $\mathbb{E}_f = 180$ GPa. The misalignment was generated by initially randomly orienting (leaning) the fibrils according to the measured thickness of zylon yarn which are relatively flat. The amount of inclination and initial fibril lengths were determined by placing them within a hypothetical (tubular) yarn domain of elliptical cross-sectional area. The cross-sectional area had a minor radius of $r = 0.000185$ m and aspect ratio of 4:1, leading to a major radius of $r = 4 \times 0.000185$ m, encompassing the fibrils shown in Fig. 4. The nodal separation distance was $h_0 = 0.000725$ m (Fig. 4). In Fig. 5, one notices that if there was no fibril misalignment, the rupture would be sudden, with far less energy absorbed (area underneath the curve). Thus, a critical feature of the upcoming overall multiscale model is the incorporation of fibril misalignment into the response function. This gives the material a more gradual, realistic, rupture behavior, which is a natural outcome of the multiscale model. The misaligned response was in excellent agreement with experimental results furnished by our industrial partner, the Boeing Company. The data is accessible to the public by making a request to the United States Federal Aviation Administration (FAA) indicating project 01-C-AW-WISU: Lightweight Ballistic Protection of Flight-Critical Components on

Commercial Aircraft Part 3: zylon Yarn Tests. Report number: DOT/FAA/AR-04/45, P3. Further data is available at http://www.me.berkeley.edu/compmat.

Remark 1. The response of a yarn can be bounded in terms of the degree of fibril misalignment. For an individual jth fibril (within a yarn) one has $U_j = \frac{L_j}{L_{j\mathrm{o}}}$, where L_j is the deformed length of the fibril, and $L_{j\mathrm{o}}$ is its original length. Explicitly, the axial stretch is (Fig. 3)

$$U_j = \frac{L_j}{L_{j\mathrm{o}}} = \frac{\sqrt{(h_0 + \Delta)^2 + d_j^2}}{\sqrt{h_0^2 + d_j^2}}, \tag{2.3}$$

where one denotes the initial nominal length between nodes (suture points) by h_0, the length of misalignment for the jth fibril within the yarn by d_j and where Δ is the displacement between two connected nodes (yarn connections). For the Ith yarn (containing N_I fibrils), the effective axial second Piola–Kirchhoff response (per yarn) can be written in terms of the fibril deformation and material properties

$$S_I = \mathbb{E}_I^* \frac{1}{2}\left(\frac{(h_0 + \Delta)^2}{h_0^2} - 1\right) = \frac{1}{N_I}\sum_{j=1}^{N_I} \mathbb{E}_{\mathrm{f}} \frac{1}{2}\left(\frac{(h_0 + \Delta)^2 + d_j^2}{h_0^2 + d_j^2} - 1\right) \frac{h_0}{(h_0^2 + d_j^2)^{\frac{1}{2}}} \xi_j, \tag{2.4}$$

where $\mathbb{E}_{\mathrm{f}}$ is the Young's modulus of a fibril, where $\mathbb{E}_I^*$ is the effective Young's modulus of the yarn, where (I) $d_j = d_0\gamma_j$, where γ is a random number such that $0 \leqslant \gamma_j \leqslant 1$, and where d_0 is the maximum horizontal inclination possible for a fibril (Fig. 4), (II) $\xi_j = 1$ if $U_j < U_{\mathrm{crit}}$ and (III) $\xi_j = 0$ if $U_j \geqslant U_{\mathrm{crit}}$ and where U_{crit} is a critical uniaxial stretch. This leads to

$$\mathbb{E}_I^* = \frac{\mathbb{E}_{\mathrm{f}} h_0^3}{N_I} \sum_{j=1}^{N_I} \frac{1}{(h_0^2 + d_j^2)^{\frac{3}{2}}} \xi_j. \tag{2.5}$$

In the absence of damage ($\xi_j = 1$, $\forall j$), the effective modulus can be bounded from below by setting $\gamma_j = 1$, $\forall j$, and above by setting $\gamma_j = 0$, $\forall j$, resulting in

$$\frac{\mathbb{E}_{\mathrm{f}} h_0^3}{(h_0^2 + d_0^2)^{\frac{3}{2}}} \leqslant \mathbb{E}_I^* \leqslant \mathbb{E}_{\mathrm{f}}. \tag{2.6}$$

The upper bound is obvious, i.e. the overall yarn stiffness can never exceed the stiffness of perfectly aligned fibrils. The lower bound indicates that, for a single yarn, the stiffness decreases in a monotone fashion with increasing fibril misalignment ($\mathcal{O}(d_0^{-3})$). We remark that, for zylon's specifications, even though the yarn is stiffer when all fibrils are aligned, the overall energy underneath the curve, for a yarn with misaligned fibrils, is larger. Further related remarks can be found in Zohdi and Steigmann [36].

Remark 2. The misaligned fibrils change their angle of inclination within the yarn, as the yarn, and hence the fibrils, stretch. They are assumed to be perfectly attached (pinned) to the suture points (nodes), which is consistent with the previously made observation that the yarn are tightly woven and that the nodes are the criss–cross (suture) contact junctions between the warp and the fill of the weave. During the macroscopic deformations, the nodes move to satisfy dynamic equilibrium, thus inducing overall nodal displacements.[4] Subsequently, the yarns, which are attached to the nodes, displace, thus changing the fibril orientation with respect to an inertial frame of reference.

[4] Later, in the large-scale computations, the nodes will correspond to the locations of lumped masses.

3. Large-scale computational methods

Clearly, if one were to attempt to compute the response for the entire network of yarn, by computing the relation in Eq. (2.5) for each yarn, *each containing hundreds of fibrils*, the computations would be highly laborious.[5] A significant reduction in the computational effort can be achieved by first precomputing the responses for a population of yarn over the entire possible deformation range, and then constructing a constitutive response with variations reflecting the approximate yarn to yarn differences.

To achieve this, the progressive damage for the Ith yarn is tracked by a single damage variable, α_I. The damage variable α_I represents the fraction of fibrils that are *not ruptured*, within the Ith yarn. Thus, for a yarn that contains no ruptured fibrils, $\alpha_I = 1$, while for an yarn that contains all ruptured fibrils, $\alpha_I = 0$. Guided by the results in Fig. 5, the mean overall stiffness of the yarn was generated to be $\mathbb{E}_y = 126$ GPa, the critical stretch, i,e, the stretch at which damage gradually starts, was set to $U_{\text{crit}} = 1.03$, which was measured by Toyobo [33]. According to the simulations of single yarn, a maximum variation of approximately $\pm 4.6\%$ in $\mathbb{E}_y$ was observed. Accordingly each yarn in the simulation was randomly assigned a value within this range.[6] Damage was approximated using the equation

$$\alpha_I(t) = \min\left(1, \alpha_I(0 \leqslant t^* < t), \frac{(\exp(-\lambda(U(t) - U_{\text{crit}})) - \exp(-0.03\lambda))}{(1 - \exp(-0.03\lambda))}\right), \tag{3.1}$$

where $U(t)$ is the stretch of the yarn at time t, and where $0 \leqslant \lambda$ is a rate parameter which is related to the amount of fibril misalignment there exists in the yarn. This relation insures that the damage always is monotonically decreasing. As $\lambda \to \infty$, the type of failure tends towards sudden rupture. As $\lambda \to 0$, there is no damage. A large number of data points were taken and then a least squares analysis was performed to arrive at a best fit value[7] of $\lambda \approx 124$.

3.1. Iterative solution procedure for fabric dynamics

For the purpose of simulating the response of initially planar networks comprised of yarn, we consider a lumped mass model, where the lumped masses are located at the suture (criss–cross) points (Fig. 3), and whereby for each lumped mass, dynamic equilibrium is computed via

$$m\ddot{\boldsymbol{u}}_i = \sum_{I=1}^{4} \boldsymbol{f}_{iI}, \tag{3.2}$$

where the four forces ($\boldsymbol{f}_{iI}$) are the axial contributions of the four yarn intersecting at node i (Fig. 3), m is the mass of a single lumped mass node, i.e. the total fabric mass divided by the total number of nodes. To determine the forces acting on a lumped mass, one simply computes the product of the Cauchy stress and the cross-sectional area. Accordingly, the contribution of the Ith yarn to the ith lumped mass is $\boldsymbol{f}_{iI} = S_I U_I A_0 \boldsymbol{a}_{iI}$ (A_0 is the cross-sectional area of yarn), where the unit axial yarn direction is given by $\boldsymbol{a}_{iI} = \frac{\boldsymbol{r}_I^+ - \boldsymbol{r}_I^-}{\|\boldsymbol{r}_I^+ - \boldsymbol{r}_I^-\|}$, where $\boldsymbol{r}_I^+$

[5] For example, consider that materials such as zylon are densely woven (35×35 yarn per square inch), with *each* yarn containing on the order of 350 fibrils, thus leading to approximately 428,750 fibrils per square inch.

[6] This accounts for the asymmetric deformation in the numerical simulations of entire sheets which come later (Fig. 7). Usually, on the order of 1000 yarn realizations are needed for adequate statistical representation, when each realization (yarn) contains on the order of 350 fibrils.

[7] With the restriction that $\alpha = 1$ when $U(t) = U_{\text{crit}}$ and $\alpha = 0$ when $U(t) = 1.06$.

denotes the endpoint not in contact with the lumped mass and $\boldsymbol{r}_I^-$ denotes the endpoint in contact with the lumped mass (Fig. 3).[8]

Clearly, $\boldsymbol{f}_{iI}$ is a function of $\boldsymbol{u}_i$. In order to handle a system such as that in Eq. (3.2), we consider the following recursive (fixed-point) scheme for all nodes $m\ddot{\boldsymbol{u}}_i^K = \sum_{I=1}^4 \boldsymbol{f}_{iI}^{K-1}$, where $K = 1, 2, 3, \ldots$ is an iteration counter. In other words, forces are first computed, then the displacements, then the forces are recomputed, etc., until a fixed-point solution, $\boldsymbol{u}^K(t + \Delta t)$, is found. Using a finite difference approximation one has $\ddot{\boldsymbol{u}}_i^K(t+\Delta t) \approx \frac{\boldsymbol{v}_i^K(t+\Delta t)-\boldsymbol{v}_i(t)}{\Delta t} \approx \frac{\boldsymbol{u}_i^K(t+\Delta t)-\boldsymbol{u}_i(t)}{(\Delta t)^2} - \frac{\boldsymbol{v}_i(t)}{\Delta t}$, leading to the following recursion relation

$$\boldsymbol{u}_i^K(t+\Delta t) = \boldsymbol{u}_i(t) + \boldsymbol{v}_i(t)\Delta t + \frac{(\Delta t)^2}{m}\sum_{I=1}^{4}\boldsymbol{f}_{iI}^{K-1}. \tag{3.3}$$

For all nodes, at a given time step, the $\boldsymbol{u}^K$ are computed until $\|\boldsymbol{u}_i^K(t+\Delta t) - \boldsymbol{u}_i^{K-1}(t+\Delta t)\| \leqslant \mathrm{TOL}$.

3.2. Convergence

Consider the general equation, $\mathscr{A}(\boldsymbol{u}) = \mathscr{F}(\boldsymbol{u})$. It is advantageous to write this in the form $\mathscr{A}(\boldsymbol{u}) - \mathscr{F}(\boldsymbol{u}) = \mathscr{G}(\boldsymbol{u}) - \boldsymbol{u} + \mathscr{E} = \boldsymbol{0}$, where $\mathscr{E} \neq \mathscr{E}(\boldsymbol{u})$ is a remainder term. A straightforward fixed-point iterative scheme is to form

$$\boldsymbol{u}^K = \mathscr{G}(\boldsymbol{u}^{K-1}) + \mathscr{E}. \tag{3.4}$$

The convergence of such a scheme is dependent on the characteristics of $\mathscr{G}$. A sufficient condition for convergence is that $\mathscr{G}$ is a contraction mapping for all $\boldsymbol{u}^K$, $K = 1, 2, 3, \ldots$ A necessary restriction for convergence is iterative self consistency, i. e. the exact solution must be reproduced by the scheme $\mathscr{G}(\boldsymbol{u}) + \mathscr{E} = \boldsymbol{u}$. Defining the error vector as $\boldsymbol{e}^K = u^K - \boldsymbol{u}$, and using the self consistency restriction, one has

$$||\boldsymbol{e}^K|| = ||\boldsymbol{u}^K - \boldsymbol{u}|| = ||\mathscr{G}(\boldsymbol{u}^{K-1}) - \mathscr{G}(\boldsymbol{u})|| \leqslant \eta^K ||\boldsymbol{u}^{K-1} - \boldsymbol{u}||. \tag{3.5}$$

Thus, if $\eta^K < 1$ for each iteration K, then $\boldsymbol{e}^K \to \boldsymbol{0}$ for any arbitrary starting solution $\boldsymbol{u}^{K=0}$ as $K \to \infty$. For the problem at hand, since $\mathscr{G}(\boldsymbol{u}_i^K) \stackrel{\mathrm{def}}{=} \frac{(\Delta t)^2}{m}\sum_{I=1}^4 \boldsymbol{f}_{iI}^K$, we have $\eta^K \propto \frac{(\Delta t)^2}{m}$. The rates of convergence of the iterative scheme are controlled by adapting the time step sizes in order to restrict η^K. For general remarks on iterative schemes of this type see Axelsson [3]. The approach can be considered as a type of staggering scheme, for example, see Doltsinis [9,10]. During the upcoming numerical simulations, the time steps were refined to insure fixed-point type convergence within each time step, as well as temporal discretization accuracy. A detailed strategy to do this is discussed, in an algorithmic context, shortly.

3.3. Penetrator/fabric interaction

A problem of interest is the resistance to puncture of initially planar sheets of fabric by a dynamic penetrator (Fig. 6). In order to simplify the problem somewhat, it is assumed that the penetrator is rigid and has only one velocity component, orthogonal (in the z-direction) to the undeformed plane of the fabric. Building on an approach developed in Zohdi [37], the velocity, directly after initial contact, can be computed from a balance of momentum in the z-direction, $m_p v_{pz}^0 = m_p v_{pz} + m_{\mathrm{f}}^{\mathrm{C}} v_{\mathrm{f}z}$, where all nodes that are underneath the penetrator are restricted to initially have the same z-component of velocity as the penetrator, however, they may slide, in a frictionless manner, in any other direction. As the simulation progresses, nodes are allowed to move beyond the penetrator, but never back through it. Here m_p is the total mass of

[8] $||\cdot||$ indicates the Euclidean norm in R^3.

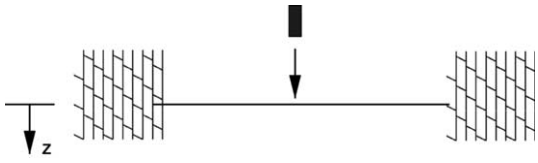

Fig. 6. A side view of a fabric–penetrator pair.

the penetrator, v_{pz}^0 is the incoming velocity of the penetrator, v_{pz} is the velocity of the penetrator directly after initial contact, $v_{\mathrm{f}z}$ is the velocity of the fabric material in the contact zone directly after initial contact and $m_{\mathrm{f}}^{\mathrm{C}}$ represents the mass of the fabric in the contact zone. The previous relation implies that $v_{pz} = \frac{m_p}{m_p + m_{\mathrm{f}}^{\mathrm{C}}} v_{pz}^0$, where all external forces are zero due to the fact that, *initially*, the fabric is unstretched. As time progresses, when the penetrator and fabric are in contact, one has an overall work–energy relation

$$\underbrace{\frac{1}{2} m_p \boldsymbol{v}_p(t) \cdot \boldsymbol{v}_p(t)}_{\text{penetrator kinetic energy}} + \underbrace{\sum_{i=1}^{N} \frac{1}{2} m \boldsymbol{v}_i(t) \cdot \boldsymbol{v}_i(t)}_{\text{fabric kinetic energy}} - \underbrace{\sum_{I=1}^{\text{YARN}} A_0 L_0 \int_{E_I(t)}^{E_I(t+\Delta t)} S_I(t)\, \mathrm{d}E_I}_{\text{work done by yarn}}$$
$$= \underbrace{\frac{1}{2} m_p \boldsymbol{v}_p(t+\Delta t) \cdot \boldsymbol{v}_p(t+\Delta t)}_{\text{penetrator kinetic energy}} + \underbrace{\sum_{i=1}^{N} \frac{1}{2} m \boldsymbol{v}_i(t+\Delta t) \cdot \boldsymbol{v}_i(t+\Delta t)}_{\text{fabric kinetic energy}}. \tag{3.6}$$

Noting that, due to the restricted (z-directional) movement of the penetrator, $\boldsymbol{v}_p \cdot \boldsymbol{v}_p = v_{pz}^2$, an approximating $v_{pz}(t+\Delta t) = \frac{u_{pz}(t+\Delta t) - u_{pz}(t)}{\Delta t}$ one obtains the following

$$u_{pz}^K(t+\Delta t) = u_{pz}(t) + \Delta t \left[v_{pz}^2(t) - \frac{2}{m_p} \sum_{I=1}^{\text{YARN}} A_0 L_0 \int_{E_I(t)}^{E_I^{K-1}(t+\Delta t)} S_I^{K-1}(t)\, \mathrm{d}E_I \right.$$
$$\left. + \frac{m}{m_p} \sum_{i=1}^{N} \boldsymbol{v}_i(t) \cdot \boldsymbol{v}_i(t) - \frac{m}{m_p} \sum_{i=1}^{N} \boldsymbol{v}_i^{K-1}(t+\Delta t) \cdot \boldsymbol{v}_i^{K-1}(t+\Delta t) \right]^{\frac{1}{2}}. \tag{3.7}$$

One obtains the solution of this problem with a fixed-point iteration, which is coupled to the fixed-point iteration of the previous section, both of which are embedded within an overall solution process involving simultaneous nodal iteration. This is discussed next.

3.4. Overall algorithm

In order to determine whether penetration has occurred, the damaged state material underneath the penetrator is needed. Penetration occurs if the material directly underneath the projectile (in the contact zone) is sufficiently degraded. This is determined by computing the average of α_I in the contact zone, and comparing it to a cut-off tolerance. The overall goal is to deliver accurate solutions where the temporal discretization accuracy dictates the upper limits on the time step size (Δt^{lim}), while the upcoming strategy refines the step size further, if necessary, to control the iterative error, which represents satisfaction of dynamic equilibrium for all of the nodes. The following algorithm is applied (until penetration occurs):

FOR A SHEET/PENETRATOR PAIR: $v_{pz} = \dfrac{m_p}{m_p + m_{\mathrm{f}}^{\mathrm{C}}} v_{pz}^0$

STEP 0: STARTING TIME STEP VALUE: $\Delta t = \Delta t^{\lim}$

($\Delta t^{\lim}$ = UPPER TIME STEP DISCRETIZATION SIZE LIMIT)

STEP I: SOLVE FOR DISPLACEMENTS VIA EQUILIBRIUM: $(K = K + 1)$

$$\boldsymbol{u}_i^K(t+\Delta t) = \boldsymbol{u}_i(t) + \boldsymbol{v}_i(t)\Delta t + \frac{(\Delta t)^2}{m}\sum_{I=1}^{4} \boldsymbol{f}_{iI}^{K-1}$$

NODES IN CONTACT ZONE:

IF $u_{iz}^K(t+\Delta t) < u_{pz}^{K-1}(t+\Delta t)$ THEN:

$$u_{iz}^K(t+\Delta t) = u_{pz}^{K-1}(t+\Delta t) \quad (\textit{ENFORCED CONTACT})$$

STEP II: SOLVE FOR AXIAL CAUCHY STRESSES: $\sigma_I^K = F_I^K S_I^{K-1}$

STEP III: COMPUTE FIBRIL RUPTURE IN EACH YARN: S_I^K

STEP IV: COMPUTE PENETRATOR POSITION:

$$u_{pz}^K(t+\Delta t) = u_{pz}(t) + \Delta t\left(v_{pz}^2(t) - \frac{2}{m_p}\sum_{I=1}^{\mathrm{YARN}} A_0 L_0 \int_{E_I(t)}^{E_I^{K-1}(t+\Delta t)} S_I^{K-1}(t)\,\mathrm{d}E_I + \frac{m}{m_p}\sum_{i=1}^{N} \boldsymbol{v}_i(t)\cdot\boldsymbol{v}_i(t) - \frac{m}{m_p}\sum_{i=1}^{N} \boldsymbol{v}_i^{K-1}(t+\Delta t)\cdot\boldsymbol{v}_i^{K-1}(t+\Delta t)\right)^{\frac{1}{2}}$$

STEP V: ERROR CHECK:

(1) $\quad ||e^K|| \stackrel{\mathrm{def}}{=} \dfrac{\sum_{i=1}^{n} ||\boldsymbol{u}_i^K(t+\Delta t) - \boldsymbol{u}_i^{K-1}(t+\Delta t)||}{\sum_{i=1}^{n} ||\boldsymbol{u}_i^K(t+\Delta t) - \boldsymbol{u}_i(t)||}$

(2) $\quad \xi^K \stackrel{\mathrm{def}}{=} \dfrac{||e^K||}{TOL}$

IF TOLERANCE MET ($\xi^K \leqslant 1$) AND $K < K_d$ THEN:

INCREMENT TIME, $t = t + \Delta t$, AND GO TO **STEP** I WITH $K = 0$ AND $\Delta t = \Delta t^{\lim}$

IF TOLERANCE NOT MET($\xi^K > 1$) AND $K = K_d$ THEN:

(1) CONSTRUCT NEW TIME STEP: $\Delta t = \dfrac{\Delta t}{\xi^K}$

(2) RESTART AT TIME $= t$ AND GO TO **STEP** I WITH $K = 0$

(3.8)

4. Numerical simulations

As in the mentioned laboratory experiments, a 50 caliber (0.0127 m or 0.5 in. in diameter) cylindrical projectile, with a mass of 0.036 kg, initially traveling at 152 m/s, was considered. An initially planar, square, fabric target of dimensions 0.076×0.076 meters (3×3 in.) was chosen. The edges were clamped. The fabric was set to have 35×35 yarn per square inch (standard zylon), with each yarn estimated to be 0.00001 m in diameter. Consequently 105×105 lumped mass nodes and $3 \times 105 \times 105 = 33{,}075$ degrees of freedom (unknowns) were needed for the computations.

Penetration was said to occur if 50% of the material in a ring around the edge of the penetrator failed, i.e. 50% of the fibrils were ruptured in that region. This cut-off was calibrated by running simulation and visually identifying when the projectile broke free. This cut-off (50%) for penetration was the only free parameter in the simulation. The total simulation time was on the order of 3 min on a standard Dell workstation. Successive sequences of the fabric deformation (lumped masses) are shown in Fig. 7. As a comparison between Figs. 7 and 2 indicates, the deformation and penetration is highly localized. The deformations in the *z-direction* magnified by a factor of 10 to aid the visualization. The overall response of the material is documented in Figs. 8 and 9. After initial contact, the penetrator's kinetic energy is transformed into fabric strain energy (Fig. 8). Initially, the penetrator slowly loses energy but, as the amount of fabric being deformed expands outward, the energy loss begins to increase. There is a kink in the plots when the fibers first begins to experience damage and the energy loss slows as the penetrator tears its way through the fabric. The fraction of fibrils that are *not ruptured* (average α) in a ring (current configuration) around the edge of the penetrator are shown in Fig. 9. Consistent with the frames in Fig. 7 and the experimental observations in Fig. 2, by comparing the plot on the left in Fig. 9 (overall damage in the sheet) to the plot on the right (damage in the contact zone), one sees that the damage is highly localized.

We remark that from Eq. (3.6), one can see that for significant kinetic energy to be lost (for t to $t + \delta t$), there must be a large amount of work done by the fibers, represented by the integral of the lefthand side of the equation, which in turn leads to large stretching and hence large amounts of damage. Thus the longer

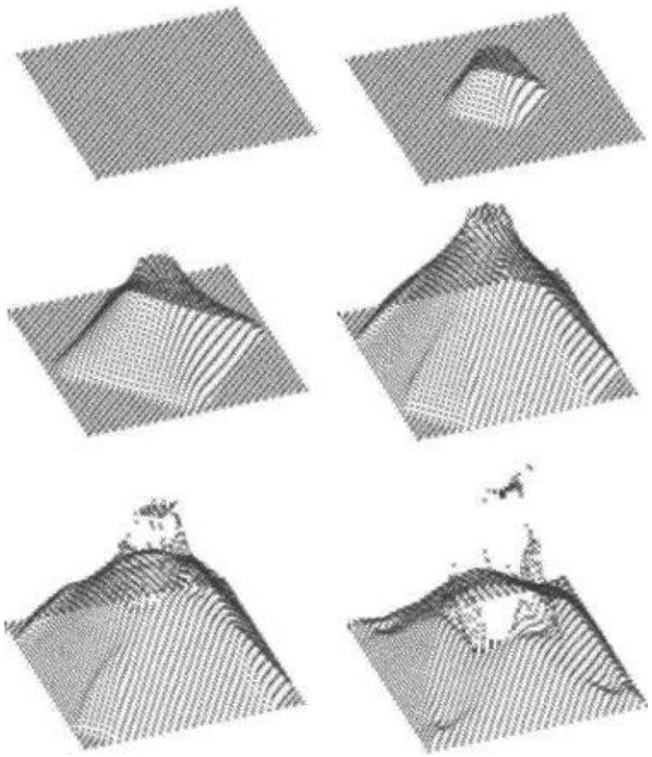

Fig. 7. Starting from the top, left to right: Successive frames of penetration leading to rupture. Not all nodes are shown for reasons of viewing clarity. The deformation in the z-direction has been magnified by a factor of 10 for easier viewing. The calculations represent the response of 11,576,250 *fibrils and* 33,075 *degrees of freedom*. Each yarn in the simulation was randomly assigned a value with the range of values discussed in the body of the paper, leading to the overall slightly asymmetric response of the fabric.

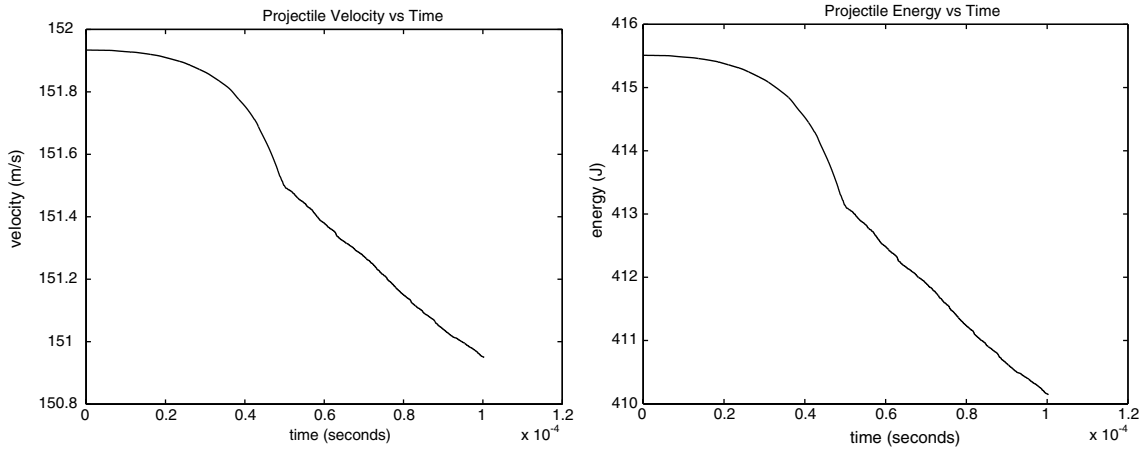

Fig. 8. Left: The velocity of the penetrator as a function of time ($v^0 = 152$ m/s). Right: The energy of the penetrator as a function of time.

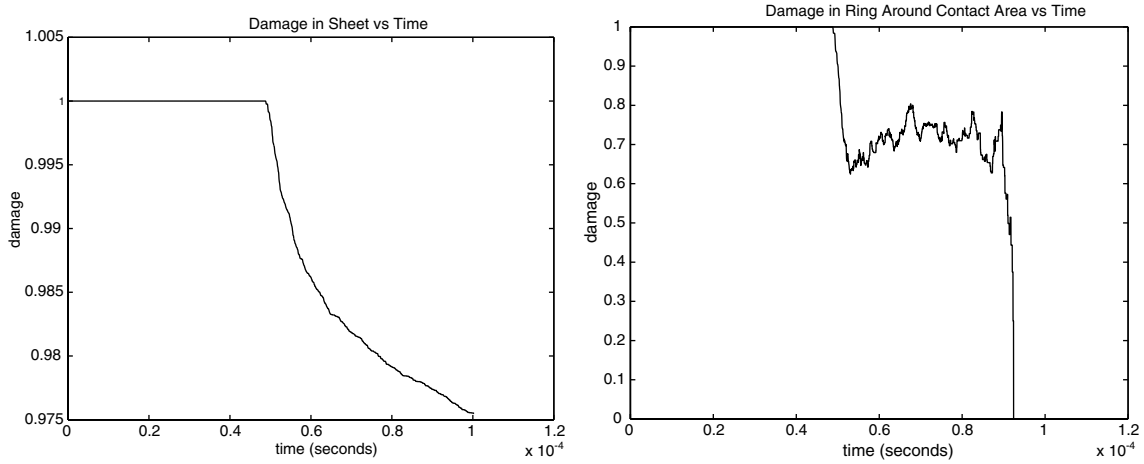

Fig. 9. Left: The fraction of fibrils that are *not ruptured* (average α) in the entire fabric sheet. Right: The average damage (α) in the contact zone.

the sheet can resist tearing, the larger the amount of deformed area and the greater the energy absorbed. It is important to emphasize that the cylindrical penetrator has *sharp edges*, and this leads to the highly localized penetration and damage. This highly localized behavior is by no mean a general trend, and occurs because of the high impact velocity and the particular penetrator shape used, in addition to the microstructure and weave specific to zylon. For more detailed studies on the various other modes of deformation, employing alternative models, we refer the reader to Lim et al. [19], Phoenix and Porwal [27] or Cheng et al. [8].

5. Summary and future work

A multiscale model was developed to describe the response of lightweight structural fabric, and an efficient numerical strategy was developed to rapidly construct and numerically simulate the multiscale system.

Large-scale simulations were conducted and compared to experimental observations. The experimental observations and simulations are qualitatively in good agreement. Calibration of the model is currently underway by making comparisons over a wide set of incoming velocities and sample sheet sizes. Independent of such calibrations, there are various improvements that can be made to address the shortcomings of the model, which would become more apparent for more complicated impact scenarios, for example with other types of penetrators. For example, the addition of friction due to fiber and yarn sliding relative to one another, which was not taken into account, is critical to capture the "combing effect" whereby the yarn and fiber become "bunched up". This is important, since, in many cases, for example when a penetrator has a tapered, ogival tip, the fabric does not rupture, but gets "combed" to the side of the penetrator. This requires a much more detailed contact analysis. Furthermore, in realistic situations, the impact will be non-standard, for example oblique. This may lead to tumbling, which requires a detailed contact analysis. Also, multiply interaction, possibly with metal layers and other fabric, is critical to describing realistic fragment barriers. For example, metal outer layers are sometimes used to blunt an initially sharp fragment, which then proceeds to be "caught" by interior fabric layers.

An important requirement of the multiscale construction is automated parameter identification. For example, parameters such as the diameter of the yarn, the damage parameter λ in Eq. (3.1) and the stiffness of the yarn are somewhat phenomenological, although we know their general character from analyses culminating in responses such as those in Fig. 5 and bounds in Eq. (2.6). This requires an inverse analysis to estimate the parameters, provided that some macroscopic test results are available. As an example, consider a cost function, denoted $\Pi(\boldsymbol{\Lambda})$, representing the response of a sheet, specifically

$$\boldsymbol{\Lambda} \stackrel{\text{def}}{=} w_1 \left| \frac{v_p(t_s) - v_p^*}{v_p^*} \right| + w_2 \left| \frac{t_s - t^*}{t_s} \right|, \tag{5.1}$$

where $v_p(t_s)$ is the velocity of the projectile at simulation time t_s and where v_p^* is the measured velocity of the projectile at time t^*. If one were to follow a standard Newton-type multivariate search to minimize Π, one would proceed by first computing a new parameter set increment, $\Delta\boldsymbol{\Lambda} = (\Delta\Lambda_1, \Delta\Lambda_2, \ldots, \Delta\Lambda_N)$, for a microstructural parameter set vector, $\boldsymbol{\Lambda}$, by solving the following system, $[\mathbb{H}]\{\Delta\boldsymbol{\Lambda}\} = -\{\boldsymbol{g}\}$. Here $[\mathbb{H}]$ is the Hessian matrix ($N \times N$), with components $H_{ij} = \frac{\partial^2 \Pi(\boldsymbol{\Lambda})}{\partial\Lambda_i \partial\Lambda_j}$, $\{\boldsymbol{g}\}$ is the gradient ($N \times 1$), with components $g_i = \frac{\partial \Pi(\boldsymbol{\Lambda})}{\partial\Lambda_i}$ and $\{\Delta\boldsymbol{\Lambda}\}$ is the parameter set increment ($N \times 1$), with components $\Delta\Lambda_i$. After the parameter set increment has been solved for, one then forms an updated parameter set vector, $\boldsymbol{\Lambda}^{\text{new}} = \boldsymbol{\Lambda}^{\text{old}} + \Delta\boldsymbol{\Lambda}$, and the process is repeated until $\Pi(\boldsymbol{\Lambda}) \leqslant \text{TOL}$. The primary difficulties with such an approach are that, typically, the objective functions of interest are nonconvex and nondifferentiable, i.e. $[\mathbb{H}]$ is not positive definite (invertible), and may not even exist, throughout the parameter set space. Because of these difficulties, classical deterministic gradient methods are simply not robust enough when they are used alone. However, they can be enhanced by first employing genetic algorithms, which are relatively insensitive to nonconvexity and nondifferentiability. Concisely, genetic algorithms are search methods based on the stochastic, biologically-inspired, processes such as reproduction, mutation and crossover. The key conceptual feature is that the parameters are represented by a genetic string, and survival of the fittest approaches are applied to a population of such strings to determine optimal parameter sets. Such methods follow from the work of Holland [15]. See Goldberg and Deb [11] for a relatively recent overview of the state of the art. Thus, it is suggested to use a two-level approach where, one first applies a genetic-type algorithm, in order to locate global minima, and then applies a gradient-based method to those regions where the objective function is locally smooth and convex, for example using computationally efficient techniques such as those found in Papadrakakis et al. [26]. The application of evolutionary computing ideas to other types of materials and structures can be found in Papadrakakis et al. [22–25], Lagaros et al. [18] and Zohdi [38,39].

Acknowledgments

The authors wish to thank graduate students Mr. Kelvin Kwong, Mr. Sean Kelly and Mr. Casey May for providing data and photographs of the experiments conducted in our laboratory at UC Berkeley, http://www.me.berkeley.edu/compmat. The authors extend special gratitude to Prof. George Johnson for his constructive comments during the preparation of this manuscript. The authors also wish to acknowledge funding from the United States Federal Aviation Administration, project 01-C-AW-WISU.

References

[1] A.A. Atai, D.J. Steigmann, On the nonlinear mechanics of discrete networks, Arch. Appl. Mech. 67 (1997) 303–319.
[2] A.A. Atai, D.J. Steigmann, Coupled deformations of elastic curves and surfaces, Int. J. Solids Struct. 35 (16) (1998) 1915–1952.
[3] O. Axelsson, Iterative Solution Methods, Cambridge University Press, 1994.
[4] H.A. Buchholdt, M. Davies, M.J.L. Hussey, The analysis of cable nets, J. Inst. Maths. Appl. 4 (1968) 339–358.
[5] H. Bufler, B. Nguyen-Tuong, On the work theorems in nonlinear network theory, Ing. Arch. 49 (1980) 275–286.
[6] M. Cannarozzi, A minimum principle for tractions in the elastostatics of cable networks, Int. J. Solids Struct. 23 (1987) 551–568.
[7] M. Cannarozzi, Stationary and extremum variational formulations for the elastostatics of cable networks, Meccanica 20 (1985) 136–143.
[8] M. Cheng, W. Chen, T. Weerasooriya, Experimental investigation of the transverse mechanical properties of a single Kevlar KM2 fiber, Int. J. Solids Struct. 41 (22–23) (2004) 6215–6232.
[9] I.St. Doltsinis, Coupled field problems-solution techniques for sequential and parallel processing, in: M. Papadrakakis (Ed.), Solving Large-scale Problems in Mechanics, 1993.
[10] I.S. Doltsinis, Solution of coupled systems by distinct operators, Engrg. Comput. 14 (1997) 829–868.
[11] D.E. Goldberg, K. Deb, Special issue on genetic algorithms, Comput. Methods Appl. Mech. Engrg. 186 (2–4) (2000) 121–124.
[12] E.M. Haseganu, D.J. Steigmann, Analysis of partly wrinkled membranes by the method of dynamic relaxation, Comput. Mech. 14 (1994) 596–614.
[13] E.M. Haseganu, D.J. Steigmann, Theoretical flexural response of a pressurized cylindrical membrane, Int. J. Solids Struct. 31 (1994) 27–50.
[14] E.M. Haseganu, D.J. Steigmann, Equilibrium analysis of finitely deformed elastic networks, Comput. Mech. 17 (1996) 359–373.
[15] J.H. Holland, Adaptation in Natural and Artificial Systems, University of Michigan Press, Ann Arbor, Mich., 1975.
[16] G.R. Johnson, S.R. Beissel, P.M. Cunniff, A computational model for fabrics subjected to ballistic impact, in: Proceedings of the 18th International Symposium on Ballistics, San Antonio, TX, 1999, pp. 962–969.
[17] M.G. Kollegal, S. Sridharan, Strength prediction of plain woven fabrics, J. Compos. Mater. 34 (2000) 240–257.
[18] N. Lagaros, M. Papadrakakis, G. Kokossalakis, Structural optimization using evolutionary algorithms, Comput. Struct. 80 (2002) 571–589.
[19] C.T. Lim, V.P. Shim, Y.H. Ng, Finite element modeling of the ballistic impact of fabric armour, Int. J. Impact Engrg. 28 (1) (2003) 13–31.
[20] P.D. Pangiotopoulos, A variational inequality approach to the inelastic stress-unilateral analysis of cable structures, Comput. Struct. 6 (1976) 133–139.
[21] M. Papadrakakis, A method for the automatic evaluation of the dynamic relaxation parameters, Comput. Methods Appl. Mech. Engrg. 25 (1980) 35–48.
[22] M. Papadrakakis, N. Lagaros, G. Thierauf, J. Cai, Advanced solution methods in structural optimisation using evolution strategies, Engrg. Comput. J. 15 (1) (1998) 12–34.
[23] M. Papadrakakis, N. Lagaros, Y. Tsompanakis, Structural optimization using evolution strategies and neutral networks, Comput. Methods Appl. Mech. Engrg. 156 (1) (1998) 309–335.
[24] M. Papadrakakis, N. Lagaros, Y. Tsompanakis, Optimization of large-scale 3D trusses using evolution strategies and neural networks, Int. J. Space Struct. 14 (3) (1999) 211–223.
[25] M. Papadrakakis, J. Tsompanakis, N. Lagaros, Structural shape optimisation using evolution strategies, Eng. Optim. 31 (1999) 515–540.
[26] M. Papadrakakis, N. Lagaros, Y. Tsompanakis, V. Plevris, Large scale structural optimization: computational methods and optimization algorithms, Arch. Comput. Methods Engrg., State of the art Reviews 8 (3) (2001) 239–301.
[27] S.L. Phoenix, P.K. Porwal, A new membrane model for the ballistic impact response and V_{50} performance of multi-ply fibrous systems, Int. J. Solids Struct. 40 (24) (2003) 6723–6765.
[28] A.C. Pipkin, The relaxed energy density for isotropic elastic membranes, IMA J. Appl. Math. 36 (1986) 297–308.

[29] D. Roylance, S.S. Wang, Penetration Mechanics of Textile Structures Ballistic Materials and Penetration Mechanics, Elsevier, 1980, pp. 273–293.
[30] V.P. Shim, V.B.C. Tan, T.E. Tay, Modelling deformation and damage characteristics of woven fabric under small projectile impact, Int. J. Impact Engrg. 16 (1995) 585–605.
[31] A. Tabiei, Y. Jiang, Woven fabric composite material model with material nonlinearity for finite element simulation, Int. J. Solids Struct. 36 (1999) 2757–2771.
[32] W.J. Taylor, J.R. Vinson, Modelling ballistic impact into flexible materials, AIAA J. 28 (1990) 2098–2103.
[33] Toyobo, PBO fiber ZYLON, Report of the Toyobo Corporation, LTD, 2001. Available from: www.toyobo.co.jp.
[34] D.J. Steigmann, Tension field theory, Proc. R. Soc. London A 429 (1990) 141–173.
[35] J.D. Walker, Constitutive model for fabrics with explicit static solution and ballistic limit, in: Proceedings of the 18th International Symposium on Ballistics, San Antonio, TX, 1999, pp. 1231–1238.
[36] T.I. Zohdi, D.J. Steigmann, The toughening effect of microscopic filament misalignment on macroscopic fabric response, Int. J. Fract. 115 (2002) L9–L14.
[37] T.I. Zohdi, Modeling and simulation of progressive penetration of multilayered ballistic fabric shielding, Comput. Mech. 29 (2002) 61–67.
[38] T.I. Zohdi, Genetic optimization of statistically uncertain microheterogeneous solids, Philos. Trans. R. Soc.: Math. Phys. Engrg. Sci. 361 (1806) (2003) 1021–1043.
[39] T.I. Zohdi, Constrained inverse formulations in random material design, Comput. Methods Appl. Mech. Engrg. 192 (28–30, 18) (2003) 3179–3194.